Functional Materials Letters
Vol. 8, No. 2 (2015) 1550030 (6 pages)

DOI: 10.1142/S1793604715500307

World Scientific
www.worldscientific.com

Structural and optical properties of KNN nanocubes synthesized by a green route using gelatin

Gh. H. Khorrami*, A. Kompany*,‡ and A. Khorsand Zak†

*Materials and Electroceramics Laboratory, Department of Physics
Faculty of Science, Ferdowsi University of Mashhad
Mashhad, Iran

†Nanotechnology Laboratory, Esfarayen University of Technology
Esfarayen, North Khorasan, Iran
‡kompany@um.ac.ir

Received 31 July 2014; Accepted 30 November 2014; Published 6 January 2014

Sodium potassium niobate nanoparticles [$(K_{0.5}Na_{0.5})NbO_3$, KNN], KNN-NPs, were synthesized using a modified sol–gel method. Structural and optical properties of the prepared samples were investigated by thermogravometric analyzer (TGA), X-ray diffraction (XRD), transmission electron microscopy (TEM), Raman and UV–Vis spectroscopy. The XRD patterns showed that the formation of the orthorhombic KNN-NPs starts at 500° C calcination temperature. Raman spectroscopy was used to investigate the crystalline symmetry and the structural deformation of the prepared KNN-NPs. TEM images showed that the morphology of the prepared particles is cubic, with the average size of about 50 nm. From diffused reflectance spectroscopy along with using Kubelka–Munk method, the energy bandgaps were determined to be indirect with the values of 3.13 eV and 3.19 eV for the samples calcined at 500° C and 600° C, respectively.

Keywords: KNN nanoparticles; structural properties; optical properties; Kubelka–Munk method.

During the last 50 years, Lead zirconate–titanate (PZT) compounds have dominated the market of piezoelectric instruments and have widely been used in fabricating many piezoelectric devices such as transducers, transformers, sensors, and actuators due to their excellent electromechanical properties.[1–4] Recently, with increasing concern on the environmental problems, it has been attempted to replace these materials by lead-free compounds, since lead is a toxic element.[1,5] Potassium sodium niobate [$(K_xNa_{1-x})NbO_3$, (KNN)] compounds have been found to be good candidates to substitute PZTs due to their high Curie temperature of over 400° C, excellent piezoelectric properties comparing to other lead-free compounds, high photocatalyst properties, and compatibility with human tissue.[6–9] $(K_xNa_{1-x})NbO_3$ is a solid solution of potassium niobate which is a ferroelectric material, whereas sodium niobate is an anti-ferroelectric, both having orthorhombic structures. KNN has the morphotropic phase boundary (MPB) at about $x = 0.5$, where its piezoelectric properties are close to PZTs.[10] However, it is difficult to obtain dense and well-sintered KNN ceramics using solid state reaction (mixed oxides method), because of its high volatility at high temperatures.[6,11] One way to solve this problem is to reduce the initial particle size of the prepared powders, because of the fact that the driving force for sintering is inversely proportional to the particle size. In addition, decreasing the particle size affects the other properties of the material such as optical and electrical, because of the appearance of quantum confinement.[6] There are several methods for the synthesis of alkali niobates nanostructure such as hydrothermal,[12,13] solvothermal,[14] coprecipitation,[15] and sol–gel.[16,17] Among these, sol–gel is mostly employed to prepare KNN powders. However, this method includes the use of alkoxides, which are expensive and should be handled with special care to avoid the rapid hydrolysis with the moisture.[1] In addition, sol–gel is rather complicated and inappropriate for the purpose of mass products.

In this research, we used a rather facile environmentally friendly synthesis route, in which the particle size is reduced. Gelatin, which is a natural polymer, was used as polymerization agent to synthesize homogenous KNN powders. Raman spectroscopy associated with X-ray diffraction (XRD) analysis has been used to investigate the crystalline symmetry and the structural deformation of the prepared samples. UV–Vis diffused reflectance spectroscopy was employed to study

‡Corresponding author.

the optical properties and to determine the type (direct or indirect) of the optical energy bandgap of the synthesized samples which, up to our knowledge, has not been used before for this purpose.

To synthesize KNN-nanoparticles (KNN-NPs), gelatin type B from bovine skin (Sigma-Aldrich) was used as a stabilizer. The starting materials were potassium nitrate (KNO_3, $\geq$ 99% purity, Sigma-Aldrich), Sodium nitrate ($NaNO_3$, $\geq$ 99% purity, Sigma-Aldrich), ammonium niobate (V) oxalate hydrate ($C_4H_4NNbO_9 \cdot xH_2O$, 99.99% purity, Sigma-Aldrich) and distilled water as the solvent. To obtain 5 g of the final product, 2.94 g potassium nitrate, 2.48 g sodium nitrate and 20.97 g ammonium niobate (V) oxalate hydrate were separately dissolved in 5 mL, 5 mL and 100 mL distilled water, respectively and then mixed together. Meanwhile, 15 g of gelatin was gradually dissolved in 100 mL distilled water at 60°C using an oil bath, while stirring, until a clear gelatin solution was obtained. Then, the stirring speed was decreased to about 50 rpm and the cations solution was slightly added to the gelatin solution. The temperature of the oil bath was kept at 80°C until a honey-like (color and viscosity) gel was obtained. The produced gel was rubbed on the inner walls of four crucibles and then calcined at three different temperatures of 450°C, 500°C and 600°C, after which a white powder was obtained.

In order to find out the lowest needed calcination temperature, the prepared gel was analyzed by thermogravometric analyzer (DTG-60/60, Shimadzu). XRD analysis (Philips, X'pert, CuKα) was used to study the lattice structure of the prepared powders. In order to investigate the crystalline symmetry and the structural deformation of the prepared samples, Raman spectrometer (Jobin Yvon Horiba HR 800UV, Ar ion laser, 514.5 nm) was employed. UV–Vis spectroscopy (Jasco, V-670) was used to determine the type and the value of the energy bandgap of the prepared samples. The morphology of the synthesized KNN-NPs was examined using transmission electron microscopy (TEM, CM120, Philips).

Figure 1 shows the TGA curve of the produced gel and its corresponding derivative. The analysis was carried out in the range of room temperature up to 800°C. A 72% of the mass loss has occured between room temperature and about 500°C. The whole mass loss region can be divided into four main parts. The first region, from room temperature to about 170°C, shows the initial loss of water (−28.28%) with the maximum weight loss rate at 150°C. The second region, 170–280°C, is related to decomposition of the organic materials (−40.83%) with a maximum rate weight loss at 238°C. The pyrochlore phase is observed in the third region between 280°C and 400°C with the maximum rate at about 307°C. The fourth region, from 400°C to about 550°C, is the main part of the curve where the formation of the perovskite structure of KNN-NPs occurs with 36.96% weight loss.[18,19]

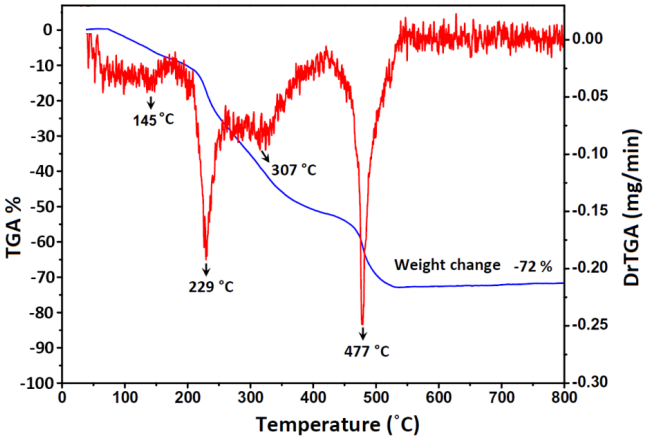

Fig. 1. TGA curve of KNN gel.

The XRD patterns of the prepared samples calcined at 450°C, 500°C and 600°C show that although some of the diffraction peaks of KNN structures are detected for the sample calcined at 450°C, formation of KNN crystalline structure is completed at 500°C, as seen in Fig. 2. Least squares refinement method was used to calculate the values of the unit cell lattice parameters and the results were found to be in accordance with the standard orthorhombic KNN pattern (JCPDS, 32-0822). The average crystallite size of the samples calcined at 500°C and 600°C were estimated using Scherrer equation ($D = \frac{k\lambda}{(\beta_{hkl} \cos\theta)}$) where, β_{hkl} is the full width half maximum (FWHM) of the (hkl) diffraction peak. The average size of the crystallites of the prepared samples was

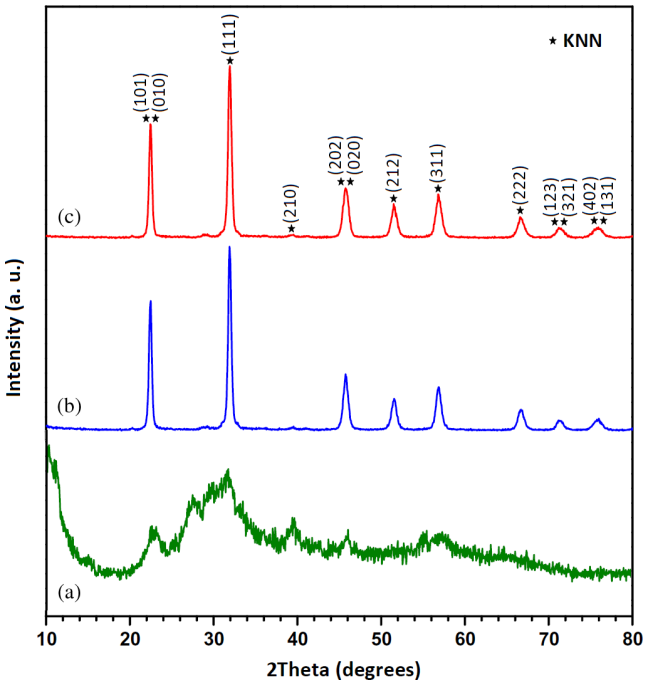

Fig. 2. XRD patterns of KNN-NPs calcined at (a) 450°C, (b) 500°C and (c) 600°C.

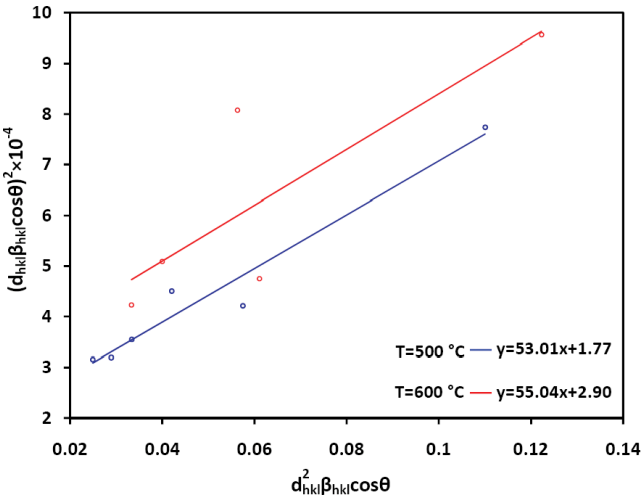

Fig. 3. SSP plots of KNN-NPs calcined at 500°C and 600°C.

obtained to be about 20 nm. It has been shown that the presence of lattice strain affects the position and broadening of the peaks in the XRD patterns.[20] So, it is more precise to consider the lattice strain for calculation of the crystallite size. For this purpose, we used size strain plot (SSP) method,[21] in which the crystallite size term is described by a Lorentzian function and the strain term by a Gaussian function.[22,23] Accordingly, we have

$$(d_{hkl}\beta_{hkl}\cos\theta)^2 = \frac{K}{D}(d^2_{hkl}\beta_{hkl}\cos\theta) + \left(\frac{\varepsilon}{2}\right)^2, \qquad (1)$$

where K is a constant that depends on the shape of the particles, and is 4/3 for spherical shape. The crystallite size and the lattice strain are obtained from the slope of the linearly fitted data and the root of the y-intercept, respectively (Fig. 3). The results are presented in Table 1. The lattice parameters of the prepared samples were calculated using Geometry equations, also presented in Table 1.

Micro-Raman spectroscopy was carried out at room temperature for the KNN-NPS calcined at 500°C and 600°C. The measurements were performed in the range of 200–1000 cm^{-1} wavenumbers. Figure 4 shows the typical vibrations corresponding to perovskite (ABO_3) structure of the prepared nanoparticles. The region with a maximum between 200 and 300 cm^{-1}, which is related to three overlapped bands that belong to the vibration modes of B_1(TO), A_1(TO) and $A_1(LO) + A_1(TO)$.[24] A weak Raman band detected at about 440 cm^{-1} corresponds to A_1(LO) vibration mode. Another broad peak which is observed between 500 cm^{-1} and 700 cm^{-1} contains two overlapped peaks at about 550 cm^{-1} and 610 cm^{-1} which are attributed to B_1(TO) and A_1(TO) modes, respectively. In addition, another peak can be observed at 860 cm^{-1}, which belongs to A_1(LO) mode. It has been reported that the vibration modes of $NaNbO_3$ are classified as NbO_6 octahedron interned modes.[25] These modes include two stretching vibrations of $A_{1g}(\nu_1)$ and $E_g(\nu_2)$, two bending vibrations ν_5 and ν_6 corresponding to F_{2g} and F_{2u} symmetries, and ν_3 and ν_4 vibrations related to F_{1u} symmetry. The same phenomena can be considered for KNN and therefore, all the observed Raman bands can be attributed to the NbO_6 octahedron vibration modes. In ABO_3 perovskite structures, the A site cations are surrounded by 12 oxygens and B (here Nb) by 6 oxygens. Therefore, the distortion depends on the size of A cation. The size of K^+ cation is larger than Na^+, thus there is less free space for NbO_6 octahedron to tilt relative to each other in the presence of K^+ instead Na^+. The smaller size of Na^+ causes an 18° tilt angle between the adjacent NbO_6 octahedron.[24] In KNN-NPs prepared at 500°C, the number of Na^+ is more than K^+ comparing to the sample calcined at 600°C, because the formation rate of $KNbO_3$ structure is lower than that of $NaNbO_3$. Therefore, the number of $KNbO_3$ is less than $NaNbO_3$ in KNN compound calcined at 500°C. However, the number of $KNbO_3$ is increased by rising the calcination temperature, which results in the shift of ν_5 and ν_6 vibrations to higher wavenumbers. In summary, by increasing the calcination temperature, $\delta \to 0$ in $K_{0.5-\delta}Na_{0.5}NbO_3$ compound. The NbO_6 octahedron modes, ν_1 and ν_2, were observed at the region between 500 cm^{-1} and 700 cm^{-1} and Nb–O vibration mode, ν_1, was detected between 850 cm^{-1} and 900 cm^{-1}.

The details of the region between 500 cm^{-1} and 700 cm^{-1} are presented in Fig. 5. The two Lorentzian peaks are attributed to $E_g(\nu_2)$ and $A_{1g}(\nu_1)$ Raman vibration modes, as indexed in Fig. 5.[26] A shift to lower wavenumbers is observed for the peak $E_g(\nu_2)$ of the sample calcined at 600°C. This shift can be due to the shortening distance of Nb^{5+} ions from its neighboring oxygen.

In order to study the optical properties of the synthesized powders, diffused reflectance measurements were carried out

Table 1. XRD analysis results of the synthesized KNN powders.

Calcination temperature (°C)	Structure	Lattice parameters			Scherrer formula	Size strain plot	
		a(Å)	b(Å)	c(Å)	Crystallite size (D) (nm)	Crystallite size (D) (nm)	Strain (ε) × 10^{-3}
500	Orthorhombic	5.57(3)	3.96(1)	5.61(0)	21.02	25.16	5.38
600	Orthorhombic	5.57(7)	3.96(2)	5.61(5)	19.79	24.24	6.78

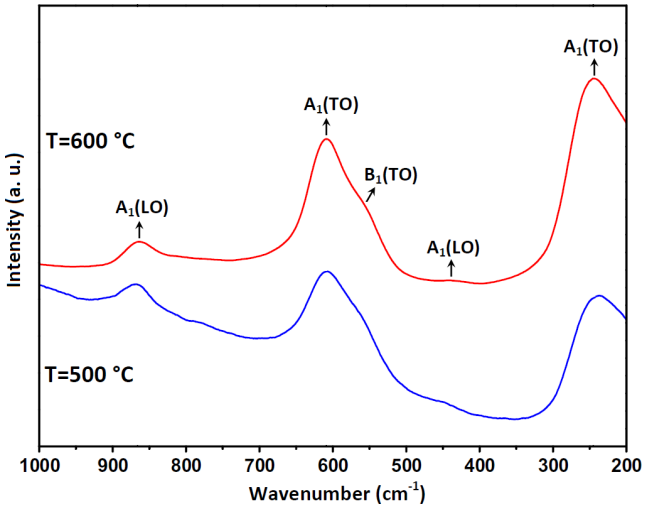

Fig. 4. Raman spectra of KNN-NPs calcined at 500°C and 600°C.

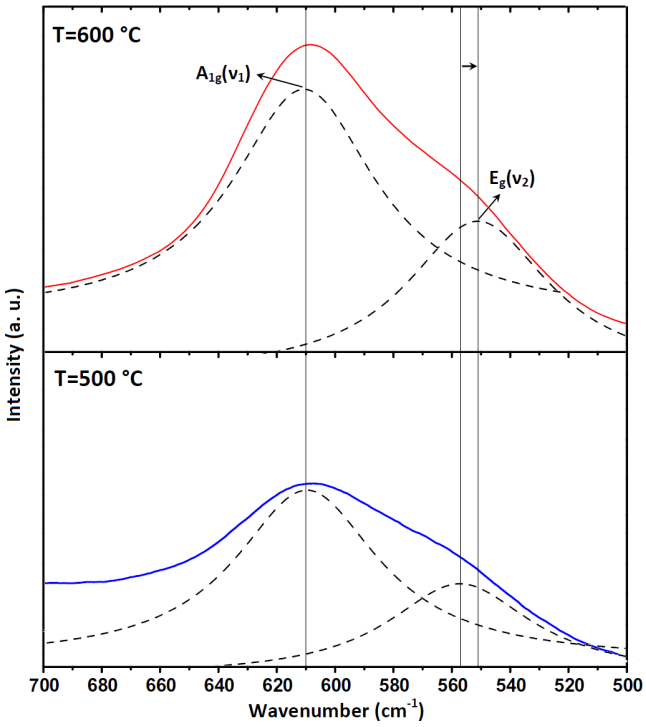

Fig. 5. Raman spectra of KNN-NPs calcined at 500°C and 600°C in the range of 500–700 wavenumbers.

in the wavelength range of 200–800 nm. It was observed that the diffused reflectance intensity is increased at about 350 nm which can be attributed to the electron transition from the valence band (O 2p) to the conduction band (Nb 4d, Fig. 6).[7,24] So, the reflectance spectra can be used to calculate the energy bandgap of the prepared samples. Normally, Kubelka–Munk method is used for this propose which is related to the Tauc relation

$$(\alpha h\nu)^{1/m} = c(h\nu - E_g), \tag{2}$$

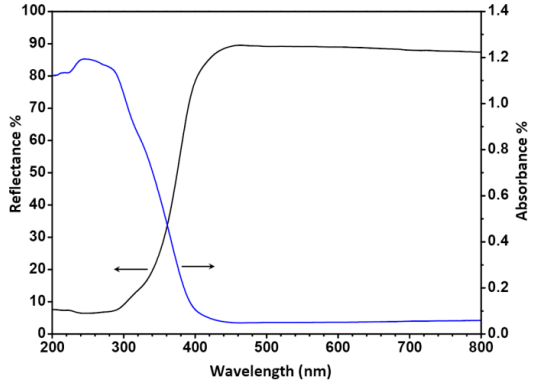

(a)

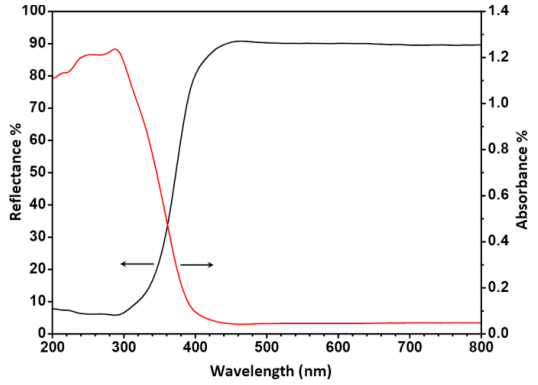

(b)

Fig. 6. UV–Vis reflectance and absorbance spectra of KNN-NPs calcined at (a) 500°C and (b) 600°C.

where α, ν, c and E_g are the absorption coefficient, light frequency, proportionality constant and the energy bandgap, respectively.[27]

In this relation, m is equal to 1/2 and 2 for direct and indirect bandgaps, respectively. The term $(\alpha h\nu)^{1/m}$ is plotted

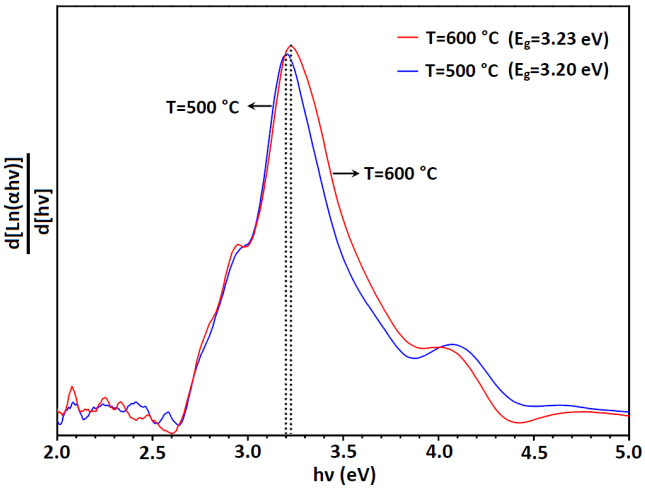

Fig. 7. The maximum of $d[\mathrm{Ln}(\alpha h\nu)]/d[h\nu]$ vs. $h\nu$ which gives the optical band gap (Eg).

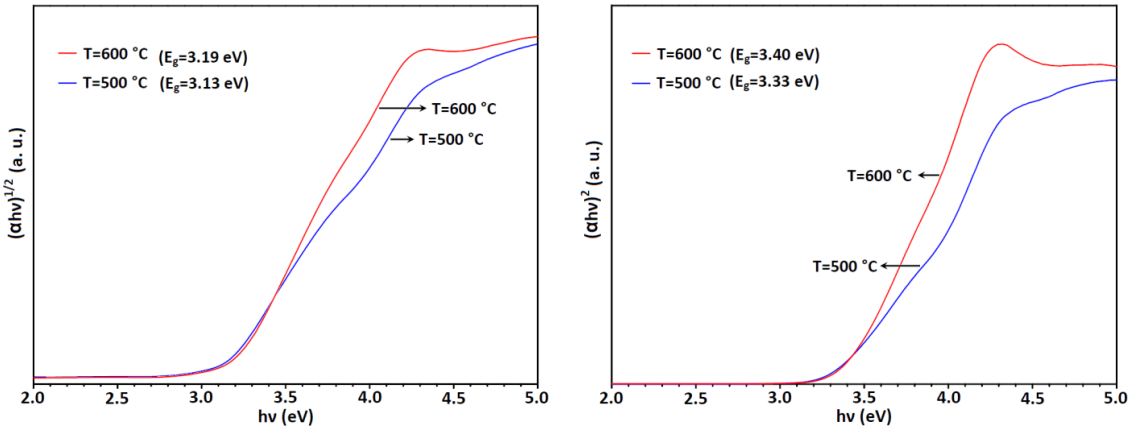

(a) (b)

Fig. 8. The optical bandgap is obtained from plotting of $(\alpha h\nu)^{1/m}$ vs. hν (a) $m = 2$ and (b) $m = 1/2$ for indirect and direct bandgaps, respectively.

Table 2. The obtained energy bandgap values of the synthesized KNN-NPs.

Calcination temperature (°C)	Bandgap (eV) (without considering m)	Indirect bandgap (eV) ($m = 2$)	Direct bandgap (eV) ($m = 1/2$)
500	3.20	3.13	3.33
600	3.23	3.19	3.40

vs. $h\nu$ and E_g can be estimated from the intersect of the slope of the curve and $h\nu$ axis. Both direct and indirect bandgaps have been reported for KNN, so it is difficult to choose the exact value of m(1/2 or 2) which must be used for the bandgap calculation process.[28] Zhao *et al.* have reported direct bandgap with 3.09 eV.[29] whereas indirect bandgap was considered for KNN by Zhou *et al.*[30] Therefore, it is better to use a different way to calculate the bandgap which does not depend on the value of m. Considering the Tauc formula, one can write:

$$\begin{aligned} \mathrm{Ln}(\alpha h\nu)^{1/m} &= \mathrm{Ln}(h\nu - E_g) \Rightarrow \mathrm{Ln}(\alpha h\nu) \\ &= m\mathrm{Ln}(h\nu - E_g) \Rightarrow \frac{d[\mathrm{Ln}(\alpha h\nu)]}{d(h\nu)} \\ &= \frac{m}{h\nu - E_g}. \end{aligned} \tag{3}$$

If the term $(d[\mathrm{Ln}(\alpha h\nu)]/d(h\nu))$ is plotted vs. $h\nu$, the obtained maximum point is related to the value of E_g, Fig. 7. Now, it is possible to find out whether the bandgap is direct or indirect, using Kubelka–Munk method in which both $m = 1/2$ and 2

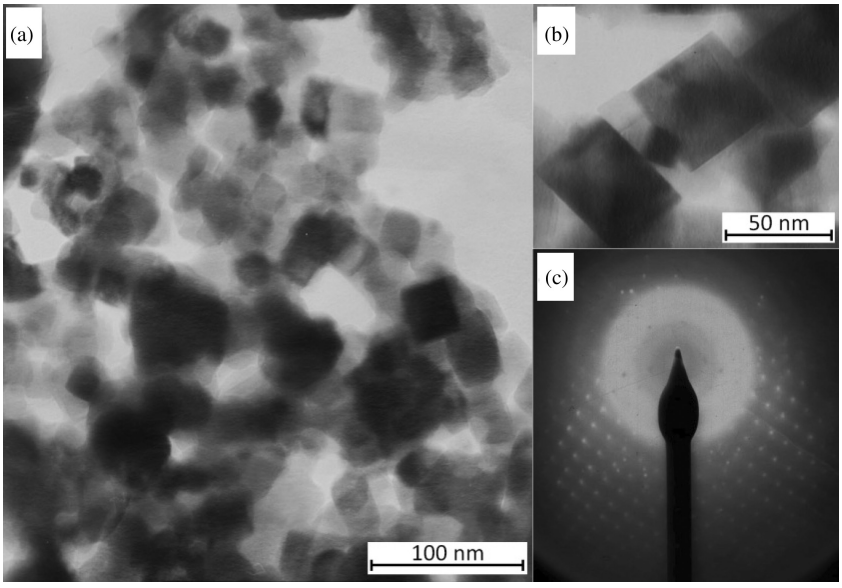

Fig. 9. (a) and (b) TEM micrographs and (c) SAED of KNN-NPs calcined at 500°C.

are employed, Fig. 8. Our results, presented in Table 2, show that the optical bandgap value obtained choosing $m = 2$ is closer to the obtained value using relation 4. Therefore, it can be concluded that the bandgap of the KNN compounds is indirect.

The TEM images of the KNN-NPs prepared at 500 are presented in Fig. 9 and the enlarged image of the particles are given in Fig. 9(b), which clearly show that the particles have grown in a cubic form with the average size of about 50 nm. Also, the selected area electron diffraction (SAED) image of the sample prepared at 500°C is shown in Fig. 9(c), which confirms the high quality of KNN-NPs synthesized by the simple method used in this work.

KNN-NPs were synthesized by a simple modified sol–gel route. The XRD patterns showed that the prepared powders have orthorhombic phase structures. The average size of the crystallites was calculated using Scherrer formula and SSP method. The crystalline symmetry and the structural deformation of the synthesized KNN-NPs were studied using Raman spectroscopy which showed that by increasing the calcination temperature, $\delta \to 0$ in $K_{0.5-\delta}Na_{0.5}NbO_3$ compound, the v_5 and v_6 vibration modes shift to higher wavenumbers. Diffused reflectance measurements were carried out in the wavelength range 200–800 nm and applying Kubelka-Munk method confirmed that the optical energy bandgap of the prepared KNN-NPs is indirect, with the value 3.13 eV and 3.19 eV for the samples calcined at 500°C and 600°C, respectively. TEM and SAED images showed that the synthesized KNN-NPs have high quality structure with the cubic shape with the average size of 50 nm.

Acknowledgments

Authors would like to thank Dr. A. Yousefi and Mrs. Moghaddam from Par-e-Tavous Research Institute-Mashhad for their assistance on TEM imaging of our samples and Mr. A. Moradi Golsheikh for the Raman spectroscopy.

References

1. R. López, F. González, M. P. Cruz and M. E. Villafuerte-Castrejon, *Mater. Res. Bullet.* **46**, 70 (2011).
2. H. Yang, Y. Lin, J. Zhu and F. Wang, *Powder Technol.* **196**, 233 (2009).
3. J. Rödel, W. Jo, K. T. P. Seifert, E. M. Anton, T. Granzow and D. Damjanovic, *J. Am. Ceramic Soc.* **92**, 1153 (2009).
4. W. Wu, M. Chen, Y. Ding and C. Liu, *J. Alloys Compounds* **588**, 496 (2014).
5. K. C. Singh, C. Jiten, R. Laishram, O. P. Thakur and D. K. Bhattacharya, *J. Alloys Compounds* **496**, 717 (2010).
6. K. C. Singh and C. Jiten, Lead-free piezoelectric ceramics manufactured from tantalum-substituted potassium sodium niobate nanopowders, *Mater. Lett.* **65**, 85 (2011).
7. R. Wang, Y. Zhu, Y. Qiu, C. F. Leung, J. He, G. Liu and T. C. Lau, *Chem. Eng. J.* **226**, 123 (2013).
8. F. Rubio-Marcos, J. J. Romero, M. S. Martín-Gonzalez and J. F. Fernández, *J. Eur. Ceramic Soc.* **30**, 2763 (2010).
9. H. Shi and Z. Zou, *J. Phys. Chem. Solids* **73**, 788 (2012).
10. P. Kumar, M. Pattanaik and S. Sharma, *Ceramics Int.* **39**, 65 (2013).
11. Y. Cao, K. Zhu, H. Zheng, J. Qiu and H. Gu, *Particuology* **10**, 777 (2012).
12. S. Li, Y. Yue, X. Ning, M. Guo and M. Zhang, *J. Alloys Compounds* **586**, 248 (2014).
13. H. Xu, M. R. Joung, J. S. Kim, S. Nahm, M. G. Kang, C. Y. Kang and S. J. Yoon, *Chem. Eng. J.* **211–212**, 16 (2012).
14. L. Li, Y. Q. Gong, L. J. Gong, H. Dong, X. F. Yi and X. J. Zheng, *Mater. Design* **33**, 362 (2012).
15. M. Pattanaik and P. Kumar, *AIP Conf. Proc.* **1313**, 284 (2010).
16. D. Q. Zhang, Z. C. Qin, X. Y. Yang, H. B. Zhu and M. S. Cao, *J. Sol–Gel Sci. Technol.* **57**, 31 (2011).
17. X. Wu, K. W. Kwok and F. Li, *J. Alloys Compounds* **580**, 88 (2013).
18. C. Wattanawikkam, N. Vittayakorn and T. Bongkarn, *Ceramics Int.* **39**, S399 (2013).
19. R. Muanghlua, S. Niemcharoen, M. Sutapun, B. Boonchom and N. Vittayakorn, *Current Appl. Phys.* **11**, 434 (2011).
20. Gh. H. Khorrami, A. Khorsand Zak, A. Kompany and R. yousefi, *Ceramics Int.* **38**, 5683 (2012).
21. Gh. H. Khorrami, A. Kompany and A. Khorsand Zak, *Modern Physics Letters B* **28**, 1450224 (2014).
22. A. Khorsand Zak, W. H. A. Majid, M. Ebrahimizadeh Abrishami, R. Yousefi and R. Parvizi, *Solid State Sci.* **14**, 488 (2012).
23. A. Khorsand Zak, W. H. Abd. Majid, M. E. Abrishami and R. Yousefi, *Solid State Sci.* **13**, 251 (2011).
24. Z. Wang, H. Gu, Y. Hu, K. Yang, M. Hu, D. Zhou and J. Guan, *CrystEngComm.* **12**, 3157 (2010).
25. Y. Shiratori, A. Magrez, J. Dornseiffer, F.-H. Haegel, C. Pithan and R. Waser, *The J. Phys. Chem. B* **109**, 20122 (2005).
26. F. Rubio-Marcos, M. A. Bañares, J. J. Romero and J. F. Fernandez, *J. Raman Spectroscopy* **42**, 639 (2011).
27. P. Li, S. Ouyang, G. Xi, T. Kako and J. Ye, *J. Phys. Chem. C* **116**, 7621 (2012).
28. J. Rani, P. K. Patel, N. Adhlakha, H. Singh, K. L. Yadav and S. Prakash, *J. Mater. Sci. Technol.*
29. P. Palei, M. Pattanaik and P. Kumar, *Ceramics Int.* **38**, 851 (2012).
30. *Chin. J. Struct. Chem.* **31**, 1095 (2012).